Shedding light on 19th century spectra by analyzing Lippmann photography

Gilles Baechler[a,1], Arnaud Latty[a], Michalina Pacholska[a], Martin Vetterli[a], and Adam Scholefield[a,1]

[a]School of Computer and Communication Sciences, Ecole Polytechnique Fédérale de Lausanne, CH-1015 Lausanne, Switzerland

Edited by David L. Donoho, Stanford University, Stanford, CA, and approved January 26, 2021 (received for review May 11, 2020)

From uncovering the structure of the atom to the nature of the universe, spectral measurements have helped some of science's greatest discoveries. While pointwise spectral measurements date back to Newton, it is commonly thought that hyperspectral images originated in the 1970s. However, the first hyperspectral images are over a century old and are locked in the safes of a handful of museums. These hidden treasures are examples of the first color photographs and earned their inventor, Gabriel Lippmann, the 1908 Nobel Prize in Physics. Since the original work of Lippmann, the process has been predominately understood from the monochromatic perspective, with analogies drawn to Bragg gratings, and the polychromatic case treated as a simple extension. As a consequence, there are misconceptions about the invertibility of the Lippmann process. We show that the multispectral image reflected from a Lippmann plate contains distortions that are not explained by current models. We describe these distortions by directly modeling the process for general spectra and devise an algorithm to recover the original spectra. This results in a complete analysis of the Lippmann process. Finally, we demonstrate the accuracy of our recovery algorithm on self-made Lippmann plates, for which the acquisition setup is fully understood. However, we show that, in the case of historical plates, there are too many unknowns to reliably recover 19th century spectra of natural scenes.

Lippmann | photography | interference | spectrography

It is often claimed that the prevalence of air travel has made the sky less blue (1). To understand whether this is true or just indulgent reminiscing, it seems natural to turn to the photographic record. While modern multispectral cameras can provide extremely accurate color information with hundreds of spectral samples taken in the visible range, most photographic techniques take just three measurements, for red, green, and blue. However, looking at the history of color photography, one early technique stands out in terms of color reproduction: Lippmann photography. While this technique is analogue, we show that it typically captures 26 to 64 spectral samples of information in the visible region, making it the earliest multispectral imaging technique.

Although the technique provides the foundations of holography and much of modern interferometric imaging, it has been almost completely forgotten today. In addition, as a photography technique, it failed to achieve mainstream adoption, mainly due to excessively long exposure times and the impossibility to create copies.

Fig. 1 shows digital images of an original Lippmann plate; one characteristic of these fascinating artworks is that the correct colors appear only under proper viewing conditions. Of course, static images do not do justice to these works and we strongly recommend that readers view a real plate, if they ever have the opportunity. In addition, we provide a video of a Lippmann plate under a moving light source, in Movie S1.

Lippmann's process works by capturing an interference pattern in a photosensitive emulsion. More precisely, during exposure, the image is focused onto a photographic plate using standard camera optics. As shown in Fig. 2, the photographic plate consists of a light-sensitive emulsion on a sheet of glass. In addition, during exposure, a mirror is created at the emulsion surface, traditionally by putting the emulsion in contact with liquid mercury. For the image acquisition, the plate is orientated such that the light from the scene passes through the glass and then the emulsion, before reflecting back from the mirror. This causes the light to interfere and the resulting interference pattern exposes the emulsion differently at different depths. For example, in the simple case of monochromatic light—that is, light made of a single wavelength—sinusoidal standing waves appear, effectively creating a Bragg grating inside the photographic emulsion.

From a chemical point of view (2), the exposure to light neutralizes some of the silver halide ions from crystal grains distributed throughout the emulsion. The reduced silver atoms form tiny metallic specks whose aggregate is called a latent image. Since silver salts are sensitive only to blue and violet light, dyes are added to the emulsion to extend the sensitivity across the full visible spectrum. In Fig. 2, we assume that the dyes are tuned to make the plate isochromatic—that is, equally sensitive to all wavelengths.

Once the plate has been exposed, it is removed from the liquid mercury and processed via standard photographic development techniques. The development is a chemical reaction that completes the reduction of silver halide into metallic silver in the exposed grains. The latent image serves as a catalyst for this reaction and thus the processed plate contains an enhanced version of the latent image. However, the enhancement is not a constant scaling of the latent image and depends on a number of characteristics of the process. For example, the developer

Significance

Gabriel Lippmann won the 1908 Nobel Prize in Physics for his method of reproducing colors in photography. Despite the significance of this result, there are still misconceptions regarding the approach. We provide a complete end-to-end analysis of the process and show, both theoretically and experimentally, how the spectrum reflected from a Lippmann plate is not the same as the exposing spectrum. In addition, we demonstrate that, given the spectrum reflected from a Lippmann plate, together with the plate's color absorption properties, the original exposing spectrum can be algorithmically recovered.

Author contributions: G.B., M.V., and A.S. designed research; G.B., A.L., M.P., and A.S. performed research; G.B. and A.L. contributed new reagents/analytic tools; G.B. and M.P. analyzed data; and G.B., A.L., M.P., M.V., and A.S. wrote the paper.

The authors declare no competing interest.

This article is a PNAS Direct Submission.

[1]To whom correspondence may be addressed. Email: gilles.baechler@gmail.com or adam.scholefield@epfl.ch.

This article contains supporting information online at https://www.pnas.org/lookup/suppl/doi:10.1073/pnas.2008819118/-/DCSupplemental.

Published April 15, 2021.

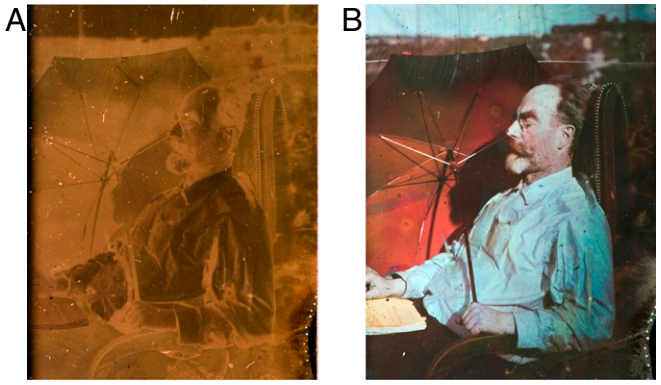

Fig. 1. Self-portrait of Gabriel Lippmann viewed under different illumination. (*A*) Diffuse illumination. (*B*) Directed light whose incoming direction is the mirror image of the viewing direction with respect to the plate's surface.

solution diffuses from the top surface of the emulsion toward the emulsion–glass interface, leading to a weaker development at deeper depths. This explains the decaying nature of the silver density in Fig. 2*C*.

Fig. 2 also shows that, before viewing, the plate is turned upside down with respect to the orientation used for exposure and the glass surface is painted black. In addition, a prism is attached to the emulsion surface with an index-matched glue—historically, Canada balsam was the adhesive of choice. To view the captured image, the plate is illuminated with a white light source. The prism separates the front surface reflection from the desired emulsion reflection and the black surface minimizes unwanted back reflections. The desired reflection from the emulsion consists of scattered light from the silver particles distributed throughout the depth of the emulsion; depending on the wavelength, the reflected light waves add more or less constructively or destructively.

Although the reproduced colors can look accurate to the eye, if we examine the full spectrum reflected from a Lippmann plate and compare it to the original, we notice a number of inconsistencies, many of which have never been documented even in modern studies (3–6). By thoroughly understanding the nature of these inconsistencies, we are able to study invertibility; i.e., given a spectrum produced by a Lippmann photograph, is it possible to undo the distortions and reconstruct the original input spectrum.

Mathematical Formulation

To understand this in more detail, consider the mathematical operators that model how the input spectrum is stored in the plate and how the developed plate synthesizes a color image (7). For simplicity, we give the equations for a single location of the image, so that the only spatial variable is z—the depth through the emulsion.

We model light fields as pulsed plane waves traveling in the direction perpendicular to the mirror. The one-dimensional (1D) wavefunction of a monochromatic light wave traveling in the positive z direction, at time t, is $U(z,t) = A\exp(j\omega t)\exp(-j\omega z/c)$. Here, j is the imaginary unit, A is the complex amplitude, c is the speed of light, and ω is the single angular frequency of the monochromatic wave. For a polychromatic spectrum, the 1D wavefunction is an infinitesimal sum of monochromatic wavefunctions: $U(z,t) = \int_0^\infty A(\omega)\exp(j\omega t)\exp(-j\omega z/c)\,d\omega$.

Exposure. During exposure, the incoming wave interferes with the reflected wave. The reflection from the mirror can be modeled as a multiplication with the mirror's reflection coefficient $r = \rho\exp(j\theta)$. Here, ρ is the attenuation factor and θ is the phase shift. As we will show, the choice of reflective medium plays a significant role in the color reproduction. The latent image—that is, the silver density after exposure—is proportional to the power of the superposed waves inside the emulsion:*

$$\begin{aligned} L(z) &\propto \int_0^\infty |A(\omega)|^2 \left|\exp\left(j\frac{\omega z}{c}\right) + r\exp\left(-j\frac{\omega z}{c}\right)\right|^2 d\omega \\ &= \int_0^\infty |A(\omega)|^2 \left(1+\rho^2+2\rho\cos\left(\frac{2\omega z}{c}-\theta\right)\right) d\omega. \end{aligned}$$

Here, we have assumed that, as depicted in Fig. 2, the reflected wave travels in the positive z direction and $z=0$ at the mirror.

Development. As previously described and depicted in Fig. 2*C*, the development enhances the silver density of the latent image differently at different depths. This can be modeled by a multiplicative function $W(z)$. This results in the following analysis operator, $\mathcal{A}$, that maps the incoming power spectrum $P(\omega) = |A(\omega)|^2$ to the developed silver density in the emulsion:

$$\mathcal{A}\{P\}(z) = W(z)\int_0^\infty P(\omega)\left(1+\rho^2+2\rho\cos\left(\frac{2\omega z}{c}-\theta\right)\right) d\omega.$$

Here, we have incorporated the unknown proportionality factor between the latent image and the power of the superposed waves into $W(z)$. In addition, $W(z)=0$ when z is outside the finite thickness of the emulsion and, due to the diffusion described previously, it decreases with increasing depth.

Viewing. The recorded silver density pattern can be thought of as elementary partially reflective mirrors, whose reflectance is proportional to the silver density after processing. When the developed plate is illuminated, the light reflected from the emulsion can be modeled as the sum of the reflections from each of these elementary partially reflective mirrors. This Born approximation neglects all but first-order reflections. It is not hard to see that such a model is not physically realistic—in particular, it assumes that all of the incoming light reaches each elementary partially reflective mirror. Despite this physical inconsistency, it is a good model for Lippmann photography because it is accurate in the regime of interest where each partially reflective mirror reflects a small amount of light.

Denote the silver density after processing by $D(z) = \mathcal{A}\{P\}(z)$ and assume that the plate is illuminated with a flat spectrum with wavefunction proportional to $\int_0^\infty \exp(j\omega t)\exp(-j\omega z/c)\,d\omega$. Then, under the previously described first-order model, the wavefunction of the light reflected from the emulsion at frequency ω is

$$U_\omega(z,t) \propto \int_0^\infty D(z')\exp(j\omega t)\exp(j\omega(z-2z')/c)\exp(j\phi)\,dz'.$$

Here, ϕ is the phase shift introduced by the reflection from any of the elementary partially reflective mirrors.

Due to the extremely short temporal period of optical waves, we observe only their power spectrum (intensity). Therefore, we define the synthesis operator, $\mathcal{S}$, as the operator that maps the silver density $D(z)$ to the power spectrum of the reflected wave. Given the previous calculations, we have for any z and t

$$\mathcal{S}\{D\}(\omega) = |U_\omega(z,t)|^2 \propto \left|\int_0^\infty D(z')\exp\left(-j\frac{2\omega z}{c}\right) dz'\right|^2.$$

*In practice, the response of a photographic plate to light is only linear in a certain regime of exposure times and intensities, the silver density reaching saturation after a certain point; its response is described by the so-called Hurter and Driffield curves (8).

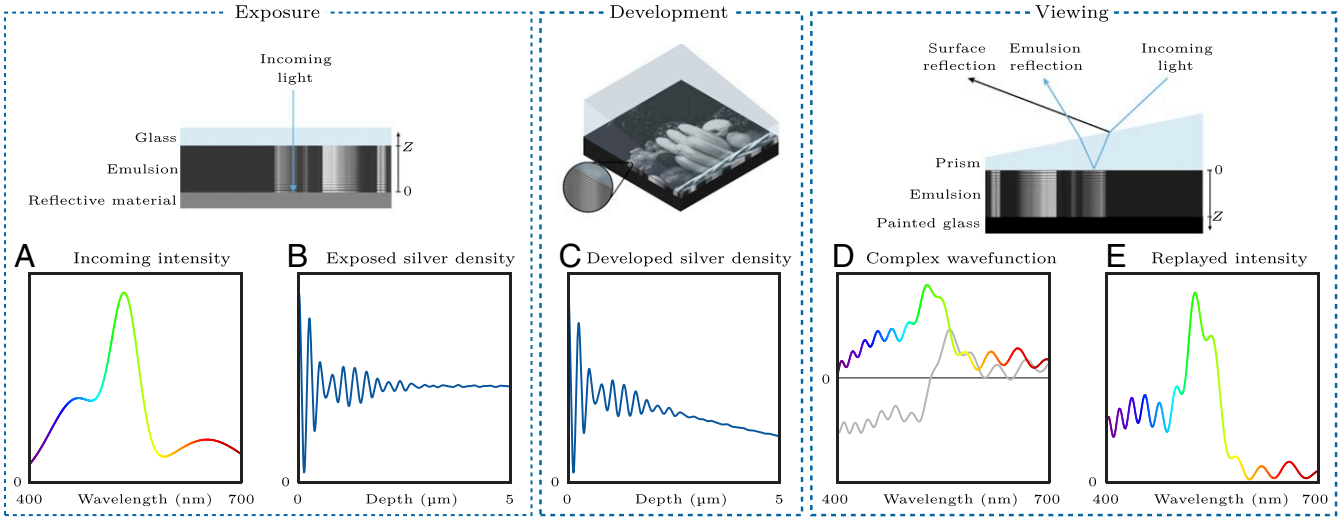

Fig. 2. Lippmann photography pipeline. (*A*) The original power spectrum incident on one spatial location of the plate, made of an emulsion layer on a glass sheet. (*B*) The silver density throughout that spatial location's depth is assumed to be proportional to the exposing interference pattern. (*C*) After exposure, the plate is developed and the silver density is multiplied by a spatial window that models development effects. (*D*) When the plate is illuminated, the light is partially reflected on each infinitesimal layer of the recorded pattern. These partial waves interfere, creating the reflected wave, which is represented by a complex wavefunction (real part in color and imaginary part in gray). (*E*) The power spectrum of the reflected wave resembles the original incoming power spectrum.

Looking at the equation, we see that the physics of the viewing process result in reflected light with frequency content proportional to the squared absolute value of the Fourier transform of the silver density.

Full pipeline. Given our modeling, the full Lippmann process consists of the composition of the analysis and synthesis operators. It can be shown that, for uniform development, this combined operator, $\mathcal{SA}$, is the following kernel operator

$$\mathcal{SA}\{P\}(\omega') \propto \left| \int_0^\infty P(\omega) H^Z(\omega, \omega') d\omega \right|^2,$$

where the kernel $H^Z(\omega, \omega')$ is

$$H^Z(\omega, \omega') = r^* S^Z(\omega' - \omega) + (1 + \rho^2) S^Z(\omega') + r S^Z(\omega' + \omega).$$

Here, $S^Z(\omega) = c\,(1 - \exp(-2jZ\omega/c))/(2j\omega)$ and Z is the thickness of the emulsion (Fig. 3).

While this formulation is not trivial, it allows us to fully model the end-to-end process of capturing and reproducing multispectral data using Lippmann's technique. In the next section, we use this modeling to show how different reflective media, emulsion thicknesses, and development properties affect the spectral reproduction. All these components play a critical role in the process and therefore cannot be ignored. Furthermore, in the commonly considered case of a perfect metallic reflector and uniform development throughout an infinitely thick plate, there are still misconceptions regarding the invertibility. For example, in this case, a common misconception is that perfect reconstruction is achieved, sometimes up to a squaring operation (6, 9); as we show, this is not true.

Results and Discussion

Choice of Reflective Medium. While standing waves are traditionally created by putting the emulsion surface in contact with liquid mercury, a simpler approach is to just let the emulsion surface make contact with the ambient air. Although the reflection is much weaker than with a metallic reflector, the refractive index change created by the emulsion–air interface creates a strong enough reflection for the process to work (10).

However, different reflective media change both the amount of light that is reflected and how the phase changes. For example, a perfect metallic mirror reflects all of the light and flips its phase (a phase shift θ of $180°$). The emulsion–mercury interface is reasonably close to this, reflecting $\rho^2 = 50.4\%$ of the light and advancing the phase by $148°$; the emulsion–air interface, on the other hand, leaves the phase unchanged and reflects 4% of the light. Clearly, this affects how the spectrum is stored in the emulsion. For example, as shown in Fig. 4*A*, the $180°$ phase shift of a perfect metallic reflection leads to minimum intensity at the mirror, whereas a dielectric reflection with no phase shift leads to maximum intensity at the same place.

Unsurprisingly, the change in silver density caused by different reflective media also affects the reflected spectrum. To demonstrate this, Fig. 4*B* shows the predicted and measured color reproduction, with both mercury and air interfaces. For the measured color reproduction, white light was dispersed through a prism and focused to produce a rainbow-colored band. A

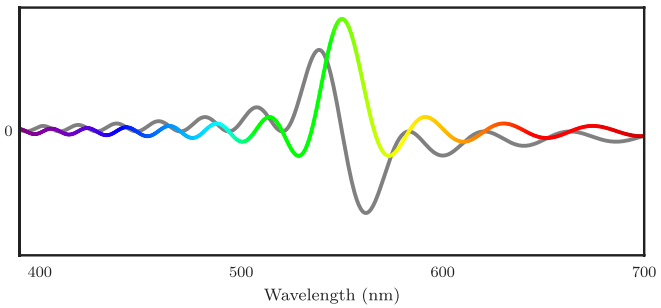

Fig. 3. The filter $S^Z(\omega' - \omega)$ for $Z = 5\mu m$ and $\omega' = \frac{2\pi c}{550nm}$. The real part is represented by the colorful line and the imaginary part by the gray line. Note that the period of the oscillations is regular with respect to the frequency ω; it appears to be changing here as we show the spectrum as a function of the wavelength, which is inversely proportional to the frequency.

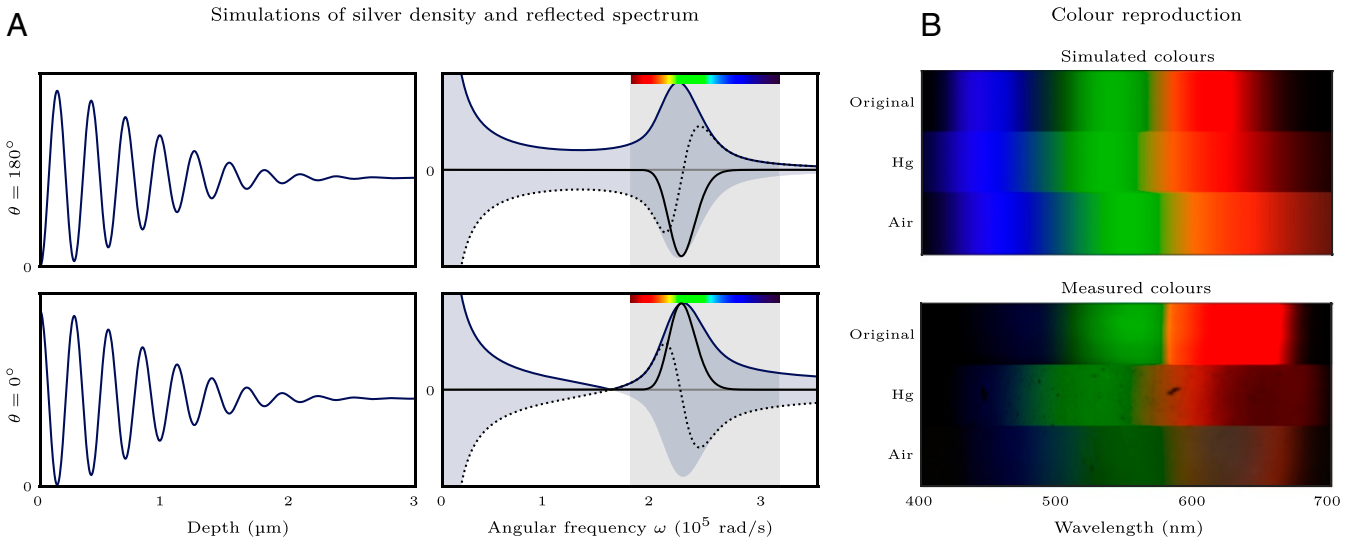

Fig. 4. The effect of the reflective medium on color reproduction. (*A*) Simulation showing how two different phase shifts at reflection lead to different interference patterns (*Left*) and reflected waves (*Right*). In the plots of the reflected waves, the real (black solid) components are the same (up to the sign), but the imaginary (dotted) components differ significantly. This leads to different skewing of the reflected power spectrum (blue solid). The skewing is toward red for $\theta = 180^\circ$ and toward blue for $\theta = 0^\circ$. (*B*) Similar effects are observed with real mirrors, both in simulations (*Top*) and in experiments (*Bottom*). In particular, reflection from mercury skews colors toward red, and reflection from air skews colors toward blue.

Lippmann plate was exposed to this rainbow, with both types of reflector, and then developed and observed. The observation was performed by photographing the plate with a color-calibrated digital single-lens reflex camera. Comparing the experiment to the model's prediction, we observe the expected shifts of the reflected spectra: For instance, green is rendered bluish with air and yellowish with mercury. We also see that bright reds are more challenging to reproduce with air, and blues are harder to represent with mercury. The dark patches in the measured colors for wavelengths greater than 600 nm occur because the plate's dyes are less sensitive to these wavelengths; we will further elaborate on the effect of dye profile when we look at spectrum recovery.

Thickness and Development of the Plate. Recall that the interference pattern is multiplied by the window function $W(z)$ to model the differing effects of the developer at different depths and the finite thickness of the emulsion. Now, since the recorded interference pattern stores low to high spectral frequencies as we move from the mirror side of the plate to the emulsion–glass interface, a finitely thick emulsion results in high spectral frequencies being clipped. Note that, by low and high spectral frequencies, we mean the slow and fast varying components of the power spectrum, not blue and red colors.

The simplest example of this is if we assume homogeneous development. In this case, $W(z)$ is a rectangle window that is zero for values of z outside the finite thickness of the emulsion and, as depicted in Fig. 5 *A3*, this results in both a smoothing of the reproduced spectrum and Gibbs ripples. These ripples provide a fingerprint of the truncation of the interference pattern and the thickness Z of the emulsion can be accurately calculated from their period $\Delta\nu$ in the frequency domain: $2Z\Delta\nu = c$.

As previously discussed, the development is not homogeneous across the emulsion, but instead is stronger closer to the surface. To model this, $W(z)$ should decay with depth. As depicted in Fig. 5 *A4* and as is well known from filter design theory (11), this damps the Gibbs ripples.

To demonstrate these effects in practice, Fig. 5 also shows electron microscope cross-section images of two plates which were exposed to monochromatic light from a laser. In addition, we show the reflected spectra of the plates. The oscillations in these spectra suggest that the plates have depths of 4.6 and 6.4 μm, which approximately match the 4.2 and 5.8 μm measured on the micrograph. In addition, the microscope images confirm the nonuniform development curve.

Finally, in Movie S2, we provide a three-dimensional reconstruction of a similar plate from ptychographic X-ray tomography at cryogenic temperature (12, 13).

Spectrum recovery. As we have seen, $\mathcal{SA} \neq I$ (I being identity) and therefore the spectrum reflected from a Lippmann plate is a distorted version of the original. A natural and interesting question to ask is whether we can find a left inverse of $\mathcal{SA}$ and thus theoretically recover the original spectrum.

Since the synthesis operator outputs a power spectrum, we lose phase information and it is not obvious that $\mathcal{SA}$ is invertible (14), even in the purely theoretical sense where everything is exactly within our model. If we also measured the phase, the combined operator $\mathcal{SA}$ would be linear and, as long as we took enough samples and restricted to a finite spectral range such as the visible spectrum, the operator could be exactly inverted with another linear operator. However, because of the loss of phase, we have to use a more advanced approach. In particular, inspired by algorithms from irregular sampling (15), we use an iterative algorithm that exploits the prior information that the true original spectrum must be a valid power spectrum. The algorithm enforces this by alternatively modifying the current estimate so that it satisfies each of the following two properties: 1) When passed through the operator $\mathcal{SA}$, it matches the measurements, and 2) it is real, positive, and does not contain frequencies corresponding to depths outside the estimated thickness of the emulsion. To enforce the second property, a nonnegative least-squares (NNLS) algorithm (16) is applied.

In terms of convergence, simulations have demonstrated that, in the noiseless case with an infinitely thick emulsion and known and invertible dye and development profiles, the proposed algorithm converges exactly to the original spectrum. Furthermore, the algorithm is robust to noise and can be modified so that, in the case of finitely thick emulsions and more general

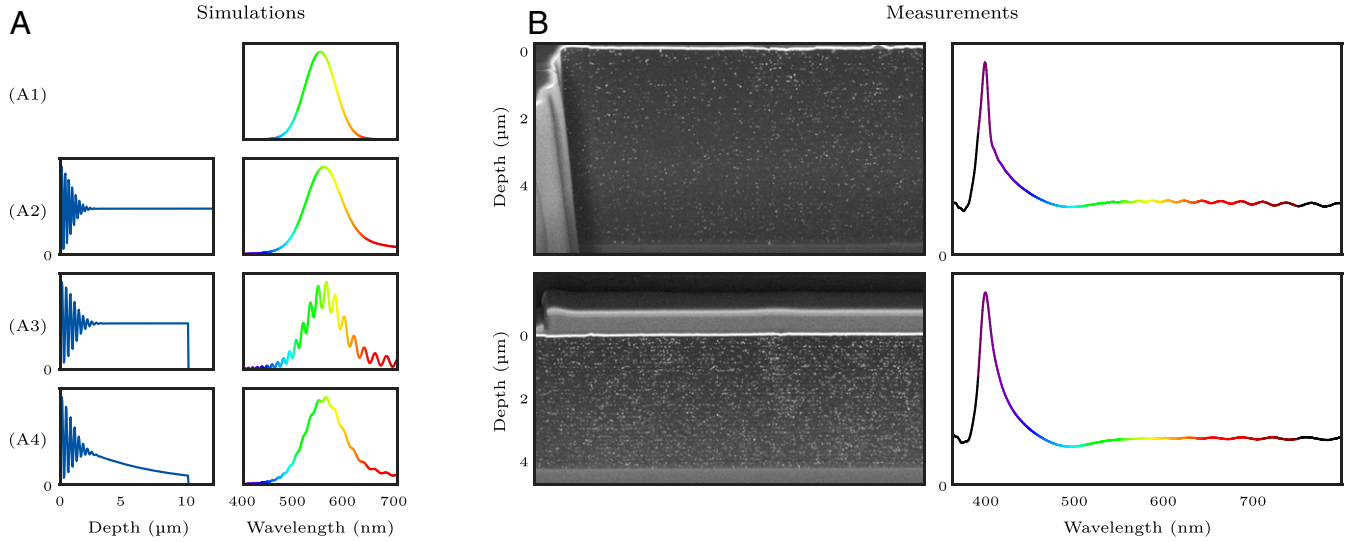

Fig. 5. The effect of the plate's thickness and development on spectrum reproduction. (*A*) Simulation of different silver density profiles (*Left*) and the corresponding reflected spectra (*Right*). (*A1*) Original spectrum. (*A2*) Infinite plate with homogeneous development: The only effect on the spectrum is the skewing described in Fig. 4. (*A3*) Finite plate with homogeneous development: Pronounced Gibbs ripples are introduced. (*A4*) Finite plate with depth-decaying development: Gibbs ripples are damped. (*B*) Electron microscope cross-sections of two plates (*Left*) and the corresponding reflected spectra (*Right*). The spectrum reflected from the thicker plate shows a higher ripple frequency.

development profiles, it recovers the best bandlimited approximation. The modification is to simply add a parametric fitting of the thickness and development parameters to the NNLS algorithm. In practice, the coherence length of the light in almost all scenes is less than the thickness of typical emulsions (4 to 10 μm), so the error from recovering only the best bandlimited approximation is negligible.

The main practical challenge comes from the dye profile (also called spectral sensitivity). In particular, our modeling up to this point has assumed that the plate is isochromatic; i.e., the dyes are such that the plate is equally sensitive to all wavelengths. When looking at color reproduction on real plates in Fig. 4, we saw that this is not the case with dark patches appearing for wavelengths greater than 600 nm. Fortunately, the analysis model can be extended to incorporate a general dye profile by simply replacing $P(\omega)$ by the product of the dye profile and the input power spectrum; however, to recover the original spectrum, the dye profile should be known and invertible.

For example, Fig. 6*A* shows a Lippmann photograph of a color checker. Since we made this photograph, we were able to measure the original spectrum of the scene, the reflected spectrum from the Lippmann plate, and the dye response of the photographic emulsion. Measurements of the original and measured spectra, as well as the estimated recovery returned by our inversion algorithm, are shown in Fig. 6. We see that the reproduction is accurate, except for regions where the dye response is weak.

Finally, in Fig. 6*B*, we present the measured and inverted spectra of four points of two historical plates. The first one (*Top*) was made by Gabriel Lippmann between 1891 and 1899 in Saas Fee, Switzerland. It thus contains century-old measurements of the spectrum of a natural scene. The second one (*Bottom*) was made by Richard Neuhauss in 1899 and is of a parrot.

Looking at the measured spectra of these historical plates, the lack of oscillations immediately stands out. From the analysis presented in Fig. 5, we know that this can be explained by a smoother decay to zero in the development window function $W(z)$. This could be due to a slightly different development or an aging effect reducing the density of silver at both boundaries of the emulsion.

In terms of spectrum recovery, unfortunately, it is impossible to measure the dye response of these plates since the dyes are washed out of the plates as part of the chemical processing. Furthermore, the dye recipes were in all probability tuned to reproduced accurate and faithful colors, rather than to achieve perfectly isochromatic solutions. Another aspect that we do not know is whether the photographers used color filters to improve the color rendition. For instance, in ref. 6, which is one of the few contemporary publications on the topic, a photo of the apparatus used to capture Lippmann photographs (with an air-based reflection) clearly shows a warming filter in front of the lens. Since they are unknown, these combined factors are unfortunately impossible to compensate for in our algorithm. Finally, it is extremely likely that the plates have been captured with mercury as a reflective medium, since they were created before E. Rothé proposed the use of air as a viable alternative (10). However, we cannot be certain about this.

Despite these limitations, we present spectrum recovery results in Fig. 6*B*, assuming uniform spectral sensitivity and a mercury reflective interface. Qualitatively, the recovered colors appear too blue, which hints that either the emulsion was not isochromatic or cooling filters were used during the capture. Another, less likely explanation is that the plates were made with air reflectors, even though they predate Rothé's publication.

Outlook

While fully modeling a Nobel Prize-winning imaging technique is of significant interest in its own right, we also believe that revisiting Lippmann's technique can inspire future technological developments in the 21st century.

For example, it could lead to future multispectral camera, printing, and display designs. On the camera front, as shown in *SI Appendix*, we have built a prototype of a digital Lippmann camera. In addition, we are particularly intrigued by the possibilities of multispectral image synthesis. In this regard, we are currently investigating printing multispectral images in glass using femtosecond lasers. The principle is almost the same as Lippmann's except that, instead of relying on photochemistry, we use

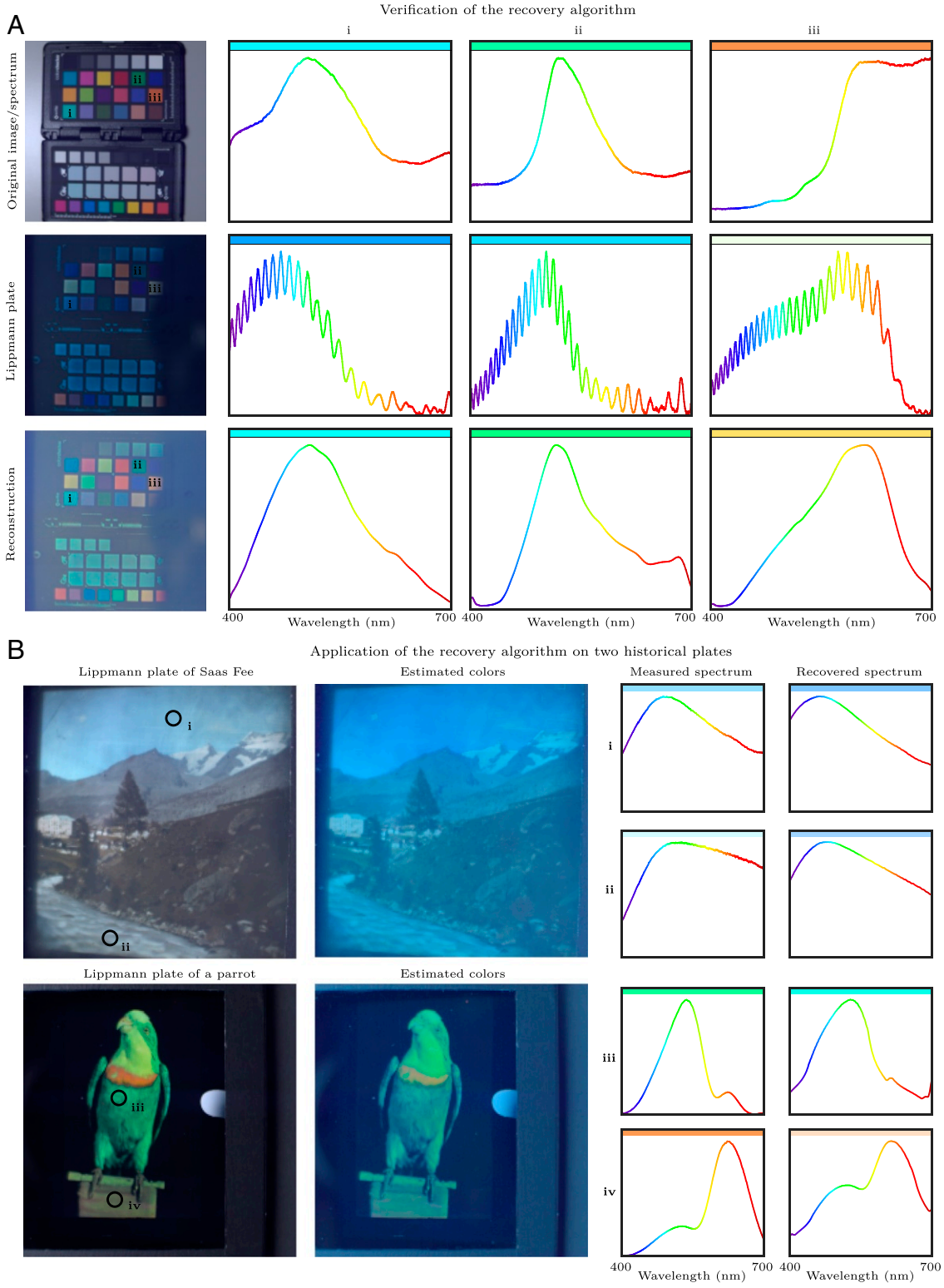

Fig. 6. Spectrum recovery. (*A*) The recovery algorithm is verified using self-made plates. (*Left*) Photographs of the color checker and of the Lippmann plate of the color checker. (*Right*) The original (*i*), measured (*ii*), and recovered (*iii*) spectra. (*B*) The recovery algorithm is applied to two historical plates. (*Left*) Photographs of the plates. (*Right*) The measured and recovered spectra.

ultrafast lasers to locally modify the refractive index of substrates such as silica (17). Since refractive index changes lead to reflections, we can, at least in principle, print Lippmann-style multispectral images at will.

Materials and Methods

To calculate the information-theoretic limit for the number of samples given in the Introduction, we note that an emulsion of finite thickness can only record spectral frequencies up to a maximal value. In addition, the

wavelengths that can be captured are also limited. For example, the glass surface of the plate prevents ultraviolet light from reaching the emulsion and the dyes are tuned to the visible spectrum, providing an infrared cutoff. Therefore, there is a finite support truncation in both mutually dual domains. Any signal with this property has only a finite number of degrees of freedom. We take this number to be the equivalent number of samples captured by the Lippmann process. To calculate it, we note that from the Nyquist–Shannon sampling formula (18), any interference pattern contained in an emulsion with thickness Z can be represented with a sampling density of $2Z/(\pi c)$ in the angular frequency domain, where c is the speed of light in the emulsion. Now, the angular frequency ω is related to the vacuum wavelength λ_0 via $\omega = 2\pi c_0/\lambda_0$, where c_0 is the speed of light in vacuum. Therefore, the equivalent number of samples over the visible spectrum for an emulsion of thickness Z is

$$\left(\frac{2\pi c_0}{\lambda_{\min}} - \frac{2\pi c_0}{\lambda_{\max}}\right) \cdot \left(\frac{2Z}{\pi c}\right) = 4Z\left(\frac{n}{\lambda_{\min}} - \frac{n}{\lambda_{\max}}\right),$$

where $\lambda_{\min}$ and $\lambda_{\max}$ are the minimum and maximum vacuum wavelengths of the visible spectrum, respectively, and n is the emulsion's refractive index. Assuming that the visible spectrum spans 400 to 700 nm, that the refractive index is 1.5, and that the emulsion thickness lies between 4 and 10 μm, we get the 26 to 64 sample range given in the Introduction.

When discussing different reflective media, we computed the amount of light reflected and phase shift for an emulsion with refractive index 1.5 at a wavelength of 589.3 nm (19).

For the color reproduction experiment of Fig. 4, a Lippmann plate was exposed to a rainbow created by decomposing white light with a prism, with an emulsion–air reflective interface. We used a U08C plate from Ultimate Holography. The plate was developed for 1 min at room temperature in a solution of distilled water and 0.83 g·L^{-1} of pyrogallol, 8.3 g·L^{-1} of potassium bromide, and 1.25 g·L^{-1} of ammonia. The plate was not fixed but a prism was added to remove the surface reflection. These choices led to the most accurate color reproduction.

For the depth experiment of Fig. 5, two plates were exposed to a 531-nm wavelength laser, with an emulsion–air reflective interface. The plates and development were the same as for the color reproduction experiment just described. However, after development, the plates were also fixed to remove the remaining silver halides, which would be otherwise confused with the metallic silver in the electron micrograph. The fixing was achieved by placing the plate in a solution of distilled water and 100 g·L^{-1} of sodium thiosulfate for 1 h at room temperature. The reflectance spectrum of each plate was measured in a vacuum to match the conditions of the subsequent microscope imaging. In addition, a prism was not added to the plates as this would prevent acquiring the same region with both techniques. Consequently, the measured spectra contain the surface reflection but this does not affect the oscillation period and thus the thickness estimation. The fixing and vacuum both lead to a shrinking of the emulsion, which explains why the peak in the spectrum has shifted toward blue, compared to the laser wavelength. The refractive index of gelatin, which is needed for thickness estimation from spectral measurement, was found to be about 1.52 by performing reflectance measurements on unexposed parts of the plates, which is in line with literature values (20). The spectral shift due to oblique incidence of the probing beam (12° from normal in air and thus 8° in emulsion) was corrected for.

For the spectrum recovery algorithm control experiment of Fig. 6*A*, an image of a color checker was made on a U08C plate with an emulsion–air reflective interface. The plate was developed as previously described but not fixed. A prism was added and the reflectance spectrum measured. The restoration algorithm was then run, taking the measured spectrum as input. The result was finally corrected for the dye sensitivity profile. This dye sensitivity was obtained using spectrometric power transmission measurements of an unexposed plate, neglecting reflection and assuming energy absorbed at any wavelength would reduce silver equally. For the spectrum recovery experiment of Fig. 6*B*, we used two historical plates from the Musée de l'Elysée. Both plates are covered with a prism, but the details of their manufacturing are unknown.

All pointwise spectral measurements were captured using a FLAME-S-XR-ES spectrometer from Ocean Optics and some custom focusing optics, such that the measured area is less than 1 mm^2. The hyperspectral images used in Fig. 6 were captured with a Specim IQ hyperspectral camera.

Data Availability. Code is available in Zenodo (https://doi.org/10.5281/zenodo.4650243) (21) and spectral measurements have been deposited in Zenodo (https://doi.org/10.5281/zenodo.4256774) (22).

ACKNOWLEDGMENTS. This work has been supported by the Swiss National Science Foundation Grant CRSII5_180232, "FemtoLippmann–Digital twin for multispectral imaging." We thank Filipe Alves for introducing us to the making of Lippmann photographs and Jean-Marc Fournier for his feedback, advice, and the many fruitful discussions. We also thank HySpex Imaging; Quantum Design; Yves Gentet from Ultimate Holography; Paolo Prandoni; Ecole Polytechnique Fédérale de Lausanne's (EPFL's) Interdisciplinary Centre for Electron Microscopy microscopy team; and the chemists Yann Pierson, Sylvain Coudret, and the Central Environmental Laboratory Group at EPFL, who have all been extremely generous with their time, equipment, and expertise. In addition, we thank and acknowledge the Paul Scherrer Institute (PSI) and in particular Mirko Holler, Elisabeth Müller, and Michal Odstrcil who prepared the sample, performed X-ray measurements, and created the three-dimensional ptychographic X-ray tomography reconstruction and rendering, shown in Movie S2. The X-ray measurements were performed at the Coherent Small-Angle X-ray Scattering beamline of the Swiss Light Source at PSI. At the Galatea laboratory, we thank Ruben Ricca, Julien Gateau, and Yves Bellouard for introducing us to material modification with ultrafast lasers—we are excited about the future of this collaboration. Last but not least, we thank Pau Maynes, Carole Sandrin, Pauline Martin, Nora Mathys, Manuel Sigrist, Sophie Ferloni, Sarah Idargo, Tatyana Franck, and the Musée de l'Elysée for their time and flexibility as well as giving us access to their collection of historical Lippmann plates, some of which are shown in Figs. 1 and 6.

1. D. J. Travis, A. M. Carleton, R. G. Lauritsen, Contrails reduce daily temperature range. *Nature* **418**, 601 (2002).
2. H. Baines, E. S. Bomback, *The Science of Photography* (Fountain Press, 1967).
3. H. Nareid, A review of the Lippmann colour process. *J. Photogr. Sci.* **36**, 140–147 (1988).
4. H. Nareid, H. M. Pedersen, Modeling of the Lippmann color process. *J. Optic. Soc. Am. A* **8**, 257–265 (1991).
5. J.-M. R. Fournier *et al.*, "Recent developments in Lippmann photography" in *SPIE 3358, Sixth International Symposium on Display Holography* (SPIE, 1998), pp. 95–102.
6. H. I. Bjelkhagen, D. Brotherton-Ratcliffe, *Ultra-Realistic Imaging: Advanced Techniques in Analogue and Digital Colour Holography* (CRC Press, 2013).
7. M. Vetterli, J. Kovačević, V. K. Goyal, *Foundations of Signal Processing* (Cambridge University Press, 2014).
8. F. Hurter, V. C. Driffield, Photochemical investigations and a new method of determination of the sensitiveness of photographic plates. *J. Soc. Chem. Indus.* **9**, 76 (1890).
9. G. Lippmann, Sur la théorie de la photographie des couleurs simples et composées par la méthode interférentielle. *J. Physique Théorique Appliquée* **3**, 97–107 (1894).
10. E. Rothé, Photographies en couleurs obtenues par la méthode interférentielle sans miroir de mercure. *Comptes Rendus Hebdomadaires à l'Académie Des Sciences* **139**, 565–567 (1904).
11. A. V. Oppenheim, R. W. Schafer, *Discrete-Time Signal Processing* (Prentice Hall Press, Upper Saddle River, NJ, ed. 3, 2009).
12. M. Holler *et al.*, OMNY PIN—a versatile sample holder for tomographic measurements at room and cryogenic temperatures. *Rev. Sci. Instrum.* **88**, 113701 (2017).
13. M. Holler *et al.*, OMNY—A tOMography Nano crYo stage. *Rev. Sci. Instrum.* **89**, 043706 (2018).
14. G. Baechler *et al.*, Super resolution phase retrieval for sparse signals. *IEEE Trans. Signal Process.* **67**, 4839–4854 (2019).
15. H. G. Feichtinger, K. Gröchenig, Theory and practice of irregular sampling. *Wavelets: Mathematics and Applications* **1994**, 305–363 (1994).
16. C. Lawson, R. Hanson, *Solving Least Squares Problems* (Society for Industrial and Applied Mathematics, 1995).
17. K. M. Davis, K. Miura, N. Sugimoto, K. Hirao, Writing waveguides in glass with a femtosecond laser. *Opt. Lett.* **21**, 1729–1731 (1996).
18. C. E. Shannon, Communication in the presence of noise. *Proc. Inst. Radio Eng.* **37**, 10–21 (1949).
19. M. Born, E. Wolf, *Principles of Optics: Electromagnetic Theory of Propagation, Interference and Diffraction of Light* (Elsevier, 2013).
20. H. I. Bjelkhagen, *Silver-Halide Recording Materials for Holography and Their Processing* (Optical Sciences, Springer-Verlag, ed. 2, 1995).
21. G. Baechler, A. Latty, A. Scholefield, M. Pacholska, Multispectral photos of Lippman plates. Zenodo. https://doi.org/10.5281/zenodo.4650243. Deposited 31 March 2021.
22. G. Baechler, M. Pacholska, A. Scholefield, A. Latty, LCAV/Lippman-photography. Zenodo. https://doi.org/10.5281/zenodo.4256774. Deposited 7 November 2020.